
Improving Generalization in Heterogeneous Federated Continual Learning via Spatio-Temporal Gradient Matching with Prototypical Coreset

Minh-Duong Nguyen[♡], Le-Tuan Nguyen[♡], Quoc-Viet Pham[♣]

[♡]Equal Contribution,

[♣]Trinity College Dublin, Ireland

{mduongbkhn, letuanhf}@gmail.com, viet.pham@tcd.ie

Abstract

Federated Continual Learning (FCL) has recently emerged as a crucial research area, as data from distributed clients typically arrives as a stream, requiring sequential learning. This paper explores a more practical and challenging FCL setting, where clients may have unrelated or even conflicting data and tasks. In this scenario, statistical heterogeneity and data noise can create spurious correlations, leading to biased feature learning and catastrophic forgetting. Existing FCL approaches often use generative replay to create pseudo-datasets of previous tasks. However, generative replay itself suffers from catastrophic forgetting and task divergence among clients, leading to overfitting in FCL. To address these challenges, we propose a novel approach called **S**patio-**T**emporal **g**radient **M**atching with network-free **P**rototype (STAMP). Our contributions are threefold: 1) We develop a model-agnostic method to determine subset of samples that effectively form prototypes when using a prototypical network, making it resilient to continual learning challenges; 2) We introduce a spatio-temporal gradient matching approach, applied at both the client-side (temporal) and server-side (spatial), to mitigate catastrophic forgetting and data heterogeneity; 3) We leverage prototypes to approximate task-wise gradients, improving gradient matching on the client-side. Extensive experiments demonstrate our method’s superiority over existing baselines.

1 Introduction

Federated Learning (FL) is a distributed and privacy-preserving approach that facilitates collaboration among various entities, such as organizations or devices (Lim et al., 2020). In FL, multiple clients train a shared model in coordination with a central server without exchanging personal data. Recently, FL has gained significant attention across multiple domains, including healthcare (Nguyen et al., 2023a), Internet-of-Things (IoT) (Nguyen et al., 2023b), and autonomous driving (Fantauzzo et al., 2022). While conventional FL studies often assume static data classes and domains, real-world scenarios involve the continuous emergence of new classes and evolving data distributions (Elsayed & Mahmood, 2024). Training entirely new models to accommodate these changes is impractical due to the substantial computational resources required. An alternative approach is transfer learning from pre-trained models; however, this method is prone to catastrophic forgetting (Dong et al., 2024), which degrades performance on previously learned classes. To address catastrophic forgetting in FL, recent research (Luo et al., 2023) has introduced the concept of Federated Continual Learning (FCL), which integrates the principles of FL and Continual Learning (CL) (Yang et al., 2023).

In FCL, clients collaboratively learn models for their private, sequential tasks while preserving data privacy. However, due to the sequential nature of these tasks, each client only has access to a

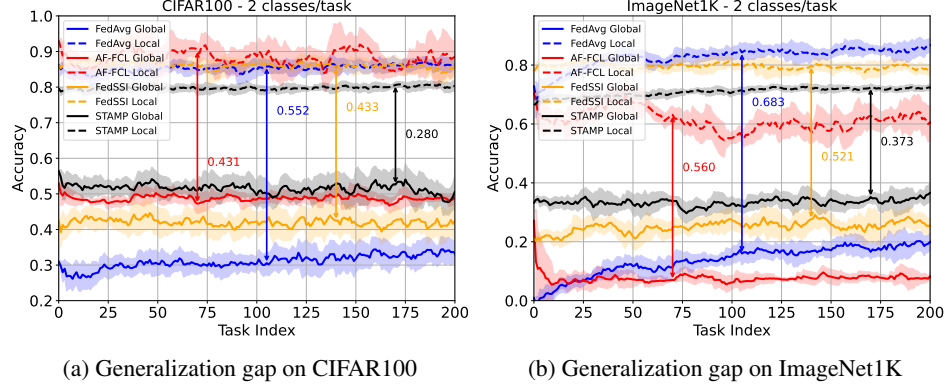


Figure 1: The illustration highlights the challenges encountered by current FCL methods (e.g., AF-FCL (Wuerkaixi et al., 2024), FedSSI (Li et al., 2025a)) when applied in heterogeneous settings. A notable gap between local and global test accuracy arises due to client-specific data heterogeneity within each task at every time step. STAMP demonstrates superior robustness over current baselines by mitigating inter-client divergence throughout the learning process, leading to a reduced local-global generalization gap.

limited amount of data from the current task. This constraint often leads to the loss of previously acquired knowledge, resulting in catastrophic forgetting. Unlike existing studies, our focus is on a more challenging setting of FCL, coined heterogeneous FCL. This setting introduces two major challenges beyond those encountered in conventional FCL. First, in heterogeneous FCL, clients are engaged in non-identical tasks at any given time, resulting in a non-uniform learning environment (see Figure 1b). As a consequence, the aggregated global model is subject to domain shifts at each communication round, impeding efficient convergence. Second, existing Federated Class-Incremental Learning (FCIL) methods perform poorly under heterogeneous FCL conditions. This is primarily because these methods typically assume a homogeneous class distribution across clients, enabling a straightforward model design where new task-specific heads are incrementally added. In contrast, heterogeneous FCL involves clients encountering different sets of classes at each task, leading to discrepancies in the architecture of local model heads. This variability substantially reduces the effectiveness of existing FCIL approaches in heterogeneous settings.

To address the aforementioned challenges, we propose a novel method, dubbed Federated Continual Learning via Spatio-Temporal gradient Matching with network-free Prototype (STAMP). Our approach offers three key contributions:

First, we apply unified gradient matching across both spatial and temporal dimensions of the FCL system. Specifically, the spatial dimension refers to task differences across clients at a given time, while the temporal dimension refers to sequential tasks within a single client. By aligning gradients across both dimensions, our method enables the identification of aggregated gradients that minimize negative transfer both across sequential tasks and between clients, thereby improving knowledge retention and overall model performance.

Second, we utilize a prototypical network to generate prototypes that serve as stable gradient approximators, even in the presence of data perturbations. This design ensures more consistent gradient estimates of previous tasks when viewed through the lens of the current model—a property often overlooked in existing gradient-based approaches (Luo et al., 2023; Lopez-Paz & Ranzato, 2017; Saha et al., 2021; Deng et al., 2021).

Third, we introduce a prototypical coreset selection strategy for efficient and robust prototype approximation. This approach offers two key advantages. (1) By carefully selecting a compact set of representative samples (coresets), our method maintains prototype quality and diversity over time with significantly reduced dependence on the prototypical networks or generative replay mechanisms used in prior work (Wei et al., 2023; Li et al., 2024a; Chen et al., 2023; Goswami et al., 2023; Qi et al., 2023; Zhen et al., 2020), both of which are prone to catastrophic forgetting in FCL settings. (2) The coreset-based strategy substantially reduces memory usage, as only a small number of representative samples per class per task are required to approximate the prototypes effectively.

2 Backgrounds & Preliminaries

2.1 Federated Continual Learning

FCL refers to a practical learning scenario that melds the principles of FL and CL. Suppose that there are U clients. On each client u , the model is trained on a sequence of T tasks. At a given step $t \times R + r$, where R represents the number of communication rounds per task and r is the current round of task t , client u holds model parameters $\theta_u^{t,r}$ and only has access to the data from task t . On client u , data \mathcal{D}_u^t of task t consists of N_u^t pairs of samples and their labels, i.e., $\mathcal{D}_u^t = \{(x_i^t, y_i^t)_{i=1}^{N_u^t}\}$.

In existing literature, the primary focus is on a specific task reshuffling setting, wherein the task set is identical for all clients, yet the arrival sequence of tasks differs (Yoon et al., 2021). In practical scenarios, it may be observed that the task set of clients is not necessarily correlated. There is no guaranteed relation among the tasks $\{\mathcal{D}_u^1, \mathcal{D}_u^2, \dots, \mathcal{D}_u^T\}$ of client u at different steps. Similarly, there is no guaranteed relation among the tasks $\{\mathcal{D}_1^t, \mathcal{D}_2^t, \dots, \mathcal{D}_U^t\}$ across different clients. Thus, we consider a more practical setting, the Limitless Task Pool (LTP).

Limitless Task Pool. In the setting of LTP, tasks are selected randomly from a substantial repository of tasks, creating a situation where two clients may not share any common tasks (i.e., $\{\mathcal{D}_u^t\}_{t=1}^{t_u} \cap \mathcal{D}_v^i\}_{i=1}^{t_v} = \emptyset, \forall u, v \in \{1, 2, \dots, U\}$). More importantly, clients possess diverse joint distributions of data and labels $p(x, y)$ due to statistical heterogeneity. Therefore, features learned from other clients could invariably introduce bias when applied to the current task of a client.

At every task t , our goal is to facilitate the collaborative construction of the global model with parameter θ^t . Under the privacy constraint inherent in FL and CL, we aim to harmoniously learn current tasks while preserving performance on previous tasks for all clients, thereby seeking to optimize performance across all tasks seen so far by all clients as follows:

$$\min_{\theta^t} [\mathcal{S}_1^t, \mathcal{S}_2^t, \dots, \mathcal{S}_U^t], \quad \text{where} \quad \mathcal{S}_u^t = [\mathcal{L}(\theta^t; \mathcal{D}_u^1), \mathcal{L}(\theta^t; \mathcal{D}_u^2), \dots, \mathcal{L}(\theta^t; \mathcal{D}_u^t)]. \quad (1)$$

However, due to the resource limitation of distributed devices, the replay memory on clients are limited. Therefore, each client u , while performing the task t , does not have access to the samples of the previously learned task $\mathcal{D}_u^{[1:t-1]}$. Therefore, the client model θ_u^t cannot be directly optimized to minimize the corresponding empirical risk $\sum_{i=1}^t \mathcal{L}(\theta_u^t; \mathcal{D}_u^i)$. Moreover, data heterogeneity on each client at specific task t introduces domain or label shifts, leading to discrepancies in data distributions across tasks and clients. This heterogeneity causes gradient conflict during training (Nguyen et al., 2025).

2.2 Gradient Matching

When learning with various non-identical tasks, gradient conflict is one of the most critical issues.

Definition 1 (Gradient conflict) *The gradient g_i and g_j ($i \neq j$) between two tasks i, j are considered to be in conflict if their cosine similarity is negative, i.e., $\cos(g_i, g_j) = \frac{g_i \cdot g_j}{|g_i| \cdot |g_j|} < 0$. In this scenario, progress along the gradient g_i results in negative transfer with respect to g_j , and vice versa.*

To mitigate the gradient conflict among tasks as in Definition 1, we leverage the Gradient Matching (GM) approach proposed in (Nguyen et al., 2025) to achieve this objective

$$\begin{aligned} \text{GM}(\mathbf{g}^{(r)}) &= \frac{\kappa \|\bar{g}^{(r)}\|}{\|\Gamma^* \mathbf{g}^{(r)}\|} \Gamma^* \mathbf{g}^{(r)} \\ \text{s.t. } \Gamma^* &= \arg \min_{\Gamma} \Gamma \mathbf{g}^{(r)} \cdot \bar{g}^{(r)} + \kappa \|\bar{g}^{(r)}\| \|g_{\Gamma}^{(r)}\|, \quad \bar{g}^{(r)} = \frac{1}{|\mathcal{T}|} \sum_{t \in \mathcal{T}} g_t^{(r)}, \end{aligned} \quad (2)$$

where $\mathbf{g}^{(r)} = [g_t^{(r)} \mid t \in \mathcal{T}]$ are the set of task-wise gradients, which participated in the training. The learned gradient $g_G = \text{GM}(\mathbf{g}^{(r)})$ utilizes the gradients of multiple tasks $\mathbf{g}^{(r)} = [g_t^{(r)} \mid t \in \mathcal{T}]$ to preserve the invariant properties of individual task-specific gradients. Specifically, since g_G satisfies the condition $g_G \cdot g_i \leq 0, \forall i \in \mathcal{T}$, it ensures that the resulting gradient does not induce negative transfer across tasks. Consequently, the aggregated gradient facilitates generalization across all tasks within the CL framework.

3 Proposed Method

We introduce a novel framework, STAMP, for heterogeneous FCL. The STAMP framework (as shown in Figure 2) comprises three key components: (1) on-client temporal gradient matching, (2) on-server spatial gradient matching, (3) replay memory with network-free prototypes.

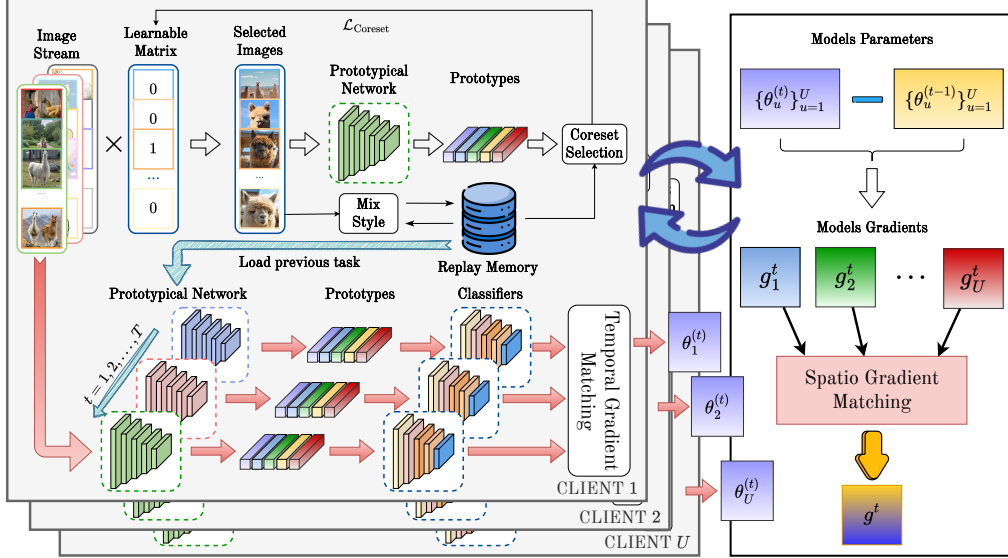


Figure 2: Illustration of STAMP architecture.

3.1 Temporal Gradient Matching

The temporal gradient matching technique is implemented on the client side in the local training. In particular, we take the gradients of previous tasks as input data for the gradient matching optimization problem as follows:

$$\theta_u^{t,r+1} = \theta_u^{t,r} - \text{GM}(\mathbf{g}_u^{[0:t]}), \quad (3)$$

where $\mathbf{g}_u^{[0:t]} = [g_u^i | i = \{1, 2, \dots, t\}]$ denotes the set of task-specific gradients, including the gradients of previous tasks $\mathbf{g}_u^{[0:t-1]}$ and current task g_u^t . Traditionally, the gradients from previous tasks are computed using stored data samples from past tasks to approximate the true gradients (Lopez-Paz & Ranzato, 2017; Luo et al., 2023; Wu et al., 2024). However, this approach requires a substantial memory buffer to store a sufficient amount of data for accurate gradient estimation. In scenarios where storage capacity is limited, the precision of the gradient approximation may be significantly compromised. An alternative solution to compute gradients is via prototype as follows:

$$g_u^{(t)} = \frac{1}{C} \sum_{c=1}^C \nabla_{\theta_u^{t,r,E}} \mathcal{L}(f(p_{u,c}^t; \theta_u^{t,r,E}); c). \quad (4)$$

To efficiently compute the prototypes for the gradient estimation, we employ the prototypical network (Snell et al., 2017). However, the prototypical network and its continual counterpart (Wei et al., 2023) may still suffer from catastrophic forgetting when deployed in the CL system. To mitigate this challenge, our intuition is to design prototypes that are learned without relying on prototype networks. To do so, we leverage a prototypical coreset which stores meaningful features for the prototype measurements in CL. The details of the prototypical coreset and its selection method are demonstrated in Section 3.3.

3.2 Spatio Gradient Matching

Building upon the work of (Nguyen et al., 2025), the spatial gradient is computed on the server to identify a consistent gradient direction that remains invariant across heterogeneous tasks in FCL. This

facilitates the global model in establishing a stable gradient direction, thereby mitigating the negative transfer that can occur due to task diversity. The update is given as follows:

$$\theta^{t,r+1} = \theta^{t,r} - \text{GM}(\mathbf{g}^t), \quad \mathbf{g}^t = [g_u^t \mid u = \{1, 2, \dots, U\}], \quad (5)$$

where \mathbf{g}^t represents the collection of local gradients obtained from the participating clients. Each local gradient is computed as $g_u^t = \theta_u^{t,r+1} - \theta_u^{t,r}$, using the model updates, and thus incurs no additional communication overhead. By aligning the gradient directions across clients, this method effectively addresses task heterogeneity, reducing the detrimental impact of client drift in heterogeneous FCL.

3.3 Prototypical Coreset assisted Replay Memory

Prototypical Coreset Selection Our primary objective is to identify salient samples within \mathcal{M}^l for each label l such that their combined representations, as processed by the encoder ϕ form a prototype on class l . To achieve this, we aim to select $|\mathcal{M}^l|$ samples from the current tasks corresponding to label l . The selected samples are then utilized to transfer information to network-free prototypes through MixStyle (Zhou et al., 2021). The selection process is defined as follows:

$$\begin{aligned} \tilde{X}^l &= \arg \min_A \left\| \left[\frac{1}{|\mathcal{M}^l|} \sum_{i \in \mathcal{M}^l} g(x_i; \phi) + \frac{1}{|\mathcal{N}_l^t|} \sum_{i \in \mathcal{N}_l^t} a_i \cdot g(x_i; \phi) \right] - p^l \right\|^2, \\ \text{s.t. } p^l &= \frac{1}{\sum_{t=1}^T |\mathcal{N}_l^t|} \left[g(\tilde{x}^l; \phi) \cdot \sum_{j=1}^{t-1} |\mathcal{N}_l^j| + \sum_{i \in \mathcal{N}_l^t} g(x_i; \phi) \right] \cdot \mathbb{1}\{y_j = l\}, \\ X^l &= \{x_i \mid a_i \in A\}, \quad X^l = K. \end{aligned} \quad (6)$$

Here, $|\mathcal{M}^l|$ is a number of samples can be stored in a replay memory according to class l and a pre-defined hyperparameter in the FCL system. Our objective is to select a set of K samples from both the network-free prototype learned from previous tasks and the newly acquired data from the current task t . If the number of selected samples exceeds K , we apply MixStyle to blend the style of the newly selected data with that of the previously identified samples, as formulated below:

$$\begin{aligned} \text{MixStyle}(\tilde{x}^l; x) &= \gamma_{\text{mix}} \frac{\tilde{x}^l - \mu(\tilde{x}^l)}{\sigma(\tilde{x}^l)} + \beta_{\text{mix}}, \\ \text{s.t. } \gamma_{\text{mix}} &= \lambda \sigma(\tilde{x}^l) + (1 - \lambda) \sigma(x), \quad \beta_{\text{mix}} = \lambda \mu(\tilde{x}^l) + (1 - \lambda) \mu(x), \end{aligned} \quad (7)$$

where x are the newly satisfying network-free prototype found from Eq. (7). To make the encoder ϕ learn the prototype better, we inherit the prototypical network (Snell et al., 2017) learning process to learn the encoder ϕ .

Prototypical Network with Coreset On each client u , the prototype $p_{u,l}^t$ on label l are computed via a prototypical network (Snell et al., 2017) via $p_{u,l}^t = \frac{1}{|\mathcal{D}_{u,l}^t|} \sum_{x_i \in \mathcal{D}_{u,l}^t} g(x_i; \phi)$. The prototypical network is learned via a loss function as follows:

$$\phi^* = \arg \min_{\phi} \sum_{l=1}^L d(g(x; \phi), p_l) + \log \sum_{l'} \exp(d(g(x; \phi), p_{l'})). \quad (8)$$

The objective of Eq. (8) is to ensure that the learned prototype $g(x; \phi)$, derived from the input data x , closely aligns with the computed prototype of the same class l across the entire batch, while simultaneously maintaining a significant distance from approximated prototypes of other classes l' .

4 Experimental Evaluations

In this section, we conduct extensive experiments to demonstrate the effectiveness of STAMP. The implementation details and additional experiments are provided in Appendices C. To ensure a fair assessment of FCL baselines under heterogeneous settings and catastrophic forgetting, we do not use pretrained models, as their training data (e.g., ImageNet1K) overlaps with our dataset, potentially biasing the evaluation.

Table 1: We report the average per-task performance of FCL under a setting where each task is assigned 20 classes. Evaluations are conducted using 10 clients (fraction = 1.0) across 5 independent trials. OOM refers to the out of memory in GPU. \uparrow and \downarrow indicate that higher and lower values are better, respectively. C \rightarrow S and S \rightarrow C denote communication from the client to the server and from the server to the client, respectively.

CIFAR100 ($U = 10, C = 20$)							
Methods	Accuracy \uparrow	AF \downarrow	Avg. Comp. \downarrow (Sec/Round)	Comm. Cost \downarrow		GPU (Peak) \downarrow	Disk \downarrow
				C \rightarrow S	S \rightarrow C		
FedAvg	27.2 (± 2.2)	5.9 (± 0.9)	27.6 sec	44.6 MB	44.6 MB	1.92 GB	N/A
FedALA	28.5 (± 2.4)	6.5 (± 1.2)	28.2 sec	44.6 MB	44.6 MB	1.93 GB	N/A
FedDBE	28.3 (± 1.6)	5.5 (± 0.7)	28.3 sec	44.6 MB	44.6 MB	1.91 GB	N/A
FedAS	40.2 (± 1.1)	30.7 (± 0.3)	135.7 sec	44.6 MB	44.6 MB	1.92 GB	N/A
FedOMG	36.8 (± 1.4)	8.5 (± 0.6)	32.7 sec	44.6 MB	44.6 MB	1.92 GB	N/A
GLFC	29.8 (± 2.1)	7.5 (± 0.4)	167.8 sec	88.2 MB	46.5 MB	3.83 GB	22.1 MB
FedCIL	32.4 (± 1.7)	6.3 (± 1.2)	199.3 sec	95.3 MB	44.6 MB	4.21 GB	18.5 MB
LANDER	45.1 (± 1.3)	5.4 (± 0.8)	153.6 sec	112.4 MB	138.7 MB	4.83 GB	131.5 MB
TARGET	32.1 (± 2.3)	5.9 (± 1.6)	236.4 sec	112.4 MB	44.6 MB	3.65 GB	18.5 MB
FedL2P	30.2 (± 1.8)	6.3 (± 1.3)	78.1 sec	56.3 MB	56.3 MB	2.56 GB	N/A
FedWeIT	37.3 (± 2.3)	4.7 (± 0.8)	38.7 sec	44.2 MB	44.2 MB	7.21 GB	N/A
AF-FCL	35.6 (± 0.4)	5.2 (± 0.5)	45.3 sec	156.3 MB	121.3 MB	8.93 GB	N/A
STAMP	41.3 (± 0.9)	5.4 (± 0.6)	56.3 sec	44.6 MB	44.6 MB	1.92 GB	16.3 MB
ImageNet1K ($U = 10, C = 20$)							
FedAvg	17.3 (± 3.3)	14.1 (± 0.2)	1485.2 sec	112.5 MB	112.5 MB	16.11 GB	N/A
FedALA	17.6 (± 5.6)	14.9 (± 0.8)	1556.6 sec	112.5 MB	112.5 MB	16.12 GB	N/A
FedDBE	18.8 (± 5.2)	13.9 (± 0.3)	1572.7 sec	112.5 MB	112.5 MB	16.11 GB	N/A
FedAS	22.3 (± 5.0)	18.2 (± 0.6)	5108.5 sec	112.5 MB	112.5 MB	16.11 GB	N/A
FedOMG	21.2 (± 3.3)	11.3 (± 0.7)	1821.2 sec	112.5 MB	112.5 MB	16.11 GB	N/A
GLFC	22.5 (± 2.1)	6.3 (± 0.2)	5647.3 sec	225.3 MB	121.2 MB	20.24 GB	112.6 MB
FedCIL	24.1 (± 2.8)	7.3 (± 0.4)	7120.3 sec	245.5 MB	112.5 MB	23.47 GB	184.3 MB
LANDER	31.8 (± 1.4)	7.8 (± 0.9)	6825.8 sec	267.4 MB	453.6 MB	26.54 GB	1.31 GB
TARGET	25.8 (± 3.8)	6.7 (± 0.4)	9958.2 sec	287.4 MB	112.5 MB	21.08 GB	184.3 MB
FedL2P	22.3 (± 3.7)	9.4 (± 0.6)	3278.7 sec	146.6 MB	146.6 MB	18.21 GB	N/A
FedWeIT	24.8 (± 1.3)	5.1 (± 0.8)	1763.8 sec	110.4 MB	110.4 MB	41.23 GB	61.7 GB
AF-FCL	21.3 (± 5.1)	4.5 (± 0.6)	1823.7 sec	421.3 MB	336.8 MB	46.81 GB	N/A
STAMP	26.8 (± 2.3)	5.8 (± 0.4)	3041.2 sec	112.5 MB	112.5 MB	16.11 GB	152.6 MB

4.1 Benchmarking with Baselines

Tables 1 and 2 report results on the CIFAR100 and ImageNet1K datasets, both featuring varying class distributions across tasks. In addition to average accuracy and average forgetting (AF), we assess key system-level metrics: computational overhead, communication cost, GPU utilization, and disk usage. Computational overhead is measured as the average time per round, reflecting the cost of client-side training, especially for generative models. Communication cost denotes the average data transferred (in GB) per client-server round. GPU utilization captures peak memory usage, critical in resource-limited settings, while disk usage reflects the total client-side storage required, including replay buffers and task-specific model parameters. The vanilla FL baselines, e.g., FedAvg, FedALA, FedAS, FedDBE, and FedOMG, may lead the model easily to forget the knowledge from past tasks, as indicated by high average forgetting. FedWeIT¹ stores task-specific head parameters in GPU memory. However, when both the number of classes (e.g., 1000 classes in ImageNet1K) and the number of tasks (e.g., 500 tasks in our ImageNet setup) become large, the total number of parameters grows significantly². As a result, storing all task-specific parameters in GPU memory

¹The official code of FedWeIT can be found at: <https://github.com/wyjeong/FedWeIT>.

²We observe from the official code that FedWeIT needs more than 512 GB of RAM memory to be able to run a simple LeNet on ImageNet. As such, we have to save the task-adaptive parameters in memory. In our reformatted implementation, we mitigate this memory constraint by utilizing disk storage for model loading.

Table 2: We report the average per-task performance of FCL under a setting where each task is assigned 2 classes. Evaluations are conducted using 10 clients (fraction = 1.0) across 5 independent trials. OOM refers to the out of memory in GPU. \uparrow and \downarrow indicate that higher and lower values are better, respectively. C \rightarrow S and S \rightarrow C denote communication from the client to the server and from the server to the client, respectively.

CIFAR100 ($U = 10, C = 2$)							
Methods	Accuracy \uparrow	AF \downarrow	Avg. Comp. \downarrow (Sec/Round)	Comm. Cost \downarrow		GPU (Peak) \downarrow	Disk \downarrow
				C \rightarrow S	S \rightarrow C		
FedAvg	31.7 (± 1.7)	25.2 (± 1.3)	3.3 sec	44.6 MB	44.6 MB	1.92 GB	N/A
FedALA	36.5 (± 2.4)	27.3 (± 0.5)	3.6 sec	44.6 MB	44.6 MB	1.93 GB	N/A
FedDBE	37.0 (± 1.6)	26.1 (± 0.7)	3.6 sec	44.6 MB	44.6 MB	1.91 GB	N/A
FedAS	58.2 (± 0.1)	56.1 (± 0.1)	13.7 sec	44.6 MB	44.6 MB	1.92 GB	N/A
FedOMG	39.1 (± 1.3)	24.5 (± 0.4)	4.1 sec	44.6 MB	44.6 MB	1.92 GB	N/A
GLFC	44.8 (± 2.1)	29.5 (± 0.4)	18.3 sec	88.2 MB	46.5 MB	4.33 GB	22.1 MB
FedCIL	46.5 (± 2.2)	28.8 (± 1.2)	22.3 sec	95.3 MB	44.6 MB	4.81 GB	18.5 MB
LANDER	50.8 (± 1.3)	22.6 (± 0.4)	15.8 sec	88.2 MB	104.3 MB	5.26 GB	131.5 MB
TARGET	45.1 (± 2.4)	28.6 (± 1.6)	25.6 sec	112.4 MB	44.6 MB	3.65 GB	18.5 MB
FedL2P	48.2 (± 1.8)	28.1 (± 0.6)	8.6 sec	56.3 MB	56.3 MB	2.56 GB	N/A
FedWeIT	52.6 (± 1.3)	25.7 (± 0.9)	5.4 sec	44.5 MB	44.5 MB	5.83 GB	61.7 GB
AF-FCL	51.4 (± 0.7)	48.7 (± 1.2)	4.9 sec	156.3 MB	121.3 MB	8.93 GB	N/A
STAMP	52.8 (± 0.9)	24.3 (± 0.8)	9.1 sec	44.6 MB	44.6 MB	1.92 GB	16.3 MB
ImageNet1K ($U = 10, C = 2$)							
FedAvg	24.3 (± 5.1)	19.6 (± 0.1)	133.2 sec	112.5 MB	112.5 MB	16.11 GB	N/A
FedALA	27.2 (± 9.1)	20.3 (± 0.2)	141.6 sec	112.5 MB	112.5 MB	16.12 GB	N/A
FedDBE	29.2 (± 7.2)	19.4 (± 0.2)	142.7 sec	112.5 MB	112.5 MB	16.11 GB	N/A
FedAS	43.5 (± 4.4)	40.2 (± 0.4)	498.5 sec	112.5 MB	112.5 MB	16.11 GB	N/A
FedOMG	30.4 (± 3.8)	21.1 (± 0.7)	171.3 sec	112.5 MB	112.5 MB	16.11 GB	N/A
GLFC	31.4 (± 3.1)	27.4 (± 0.6)	466.7 sec	225.3 MB	121.2 MB	20.24 GB	112.6 MB
FedCIL	33.8 (± 3.6)	25.8 (± 0.7)	652.3 sec	245.5 MB	112.5 MB	23.47 GB	184.3 MB
LANDER	34.9 (± 2.7)	26.1 (± 0.9)	573.8 sec	573.8 sec	453.6 MB	26.54 GB	1.31 GB
TARGET	33.2 (± 4.2)	25.2 (± 0.4)	913.2 sec	287.4 MB	112.5 MB	21.08 GB	184.3 MB
FedL2P	34.5 (± 4.8)	26.4 (± 0.2)	303.7 sec	146.6 MB	146.6 MB	18.21 GB	N/A
FedWeIT	39.7 (± 3.1)	21.5 ($\pm -$)	194.2 sec	111.8 MB	111.8 MB	62.7 GB	640 GB
AF-FCL	8.3 (± 5.3)	46.6 (± 0.3)	176.7 sec	421.3 MB	336.8 MB	46.81 GB	N/A
STAMP	41.5 (± 2.4)	24.2 (± 0.8)	321.2 sec	112.5 MB	112.5 MB	16.11 GB	152.6 MB

becomes infeasible, and they must instead be saved to disk. However, this approach leads to a substantial increase in average training time. LANDER stores all generated pseudo task-specific data on disk, incurring client-side storage overhead comparable to conventional CL methods using replay memory. Additionally, broadcasting synthetic data from the server to clients introduces substantial communication overhead.

The key observations from Tables 1 and 2 indicate that more challenging settings—specifically, those with only two classes per task—exhibit greater susceptibility to catastrophic forgetting. This is because each task provides less comprehensive information about the overall dataset, thereby leading to a higher average forgetting (AF) score. STAMP demonstrates the most substantial improvements in two key metrics: accuracy and forgetting. Moreover, its communication cost remains comparable to that of standard FL. Additionally, STAMP requires relatively modest RAM and disk resources, making it suitable for deployment on resource-constrained devices.

4.2 Performance under tasks with non-IID settings

Figure 3 illustrates the test accuracy across varying levels of data heterogeneity for CIFAR10, CIFAR100, Digit10, and Office31 datasets. As shown in the figure, all methods improve test accuracy as data heterogeneity decreases (i.e., larger α). Notably, STAMP consistently achieves superior and

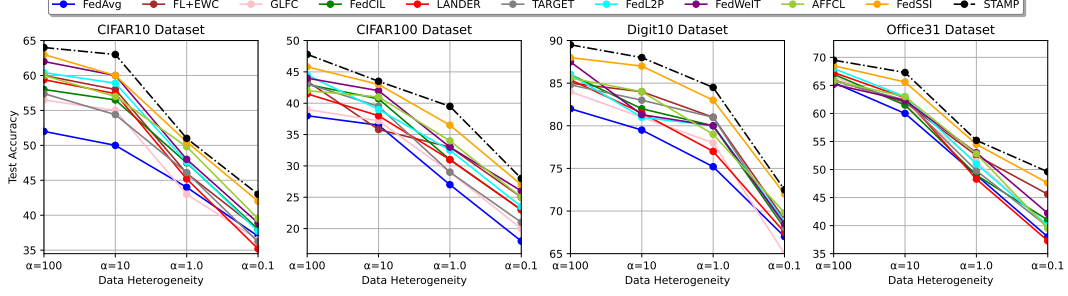


Figure 3: Performance w.r.t data heterogeneity α for four datasets.

stable performance across different levels of heterogeneity, indicating its robustness under non-IID conditions.

4.3 Analysis on STAMP

4.3.1 Efficiency of Prototypical Coreset

To evaluate the effectiveness of our proposed coreset selection method, we compare STAMP with a vanilla FL framework incorporating alternative data condensation techniques on the client side, including SRe²L (Yin et al., 2023), BCSR (Hao et al., 2023), and OCS (Yoon et al., 2022), CSReL (Tong et al., 2025). The experimental results in Figure 4 show that our method consistently outperforms these coreset selection-based FL algorithms. Notably, our approach can reduce the coreset size to as few as 20 images per class without significantly compromising performance compared to training on the full-scale dataset for previous tasks.

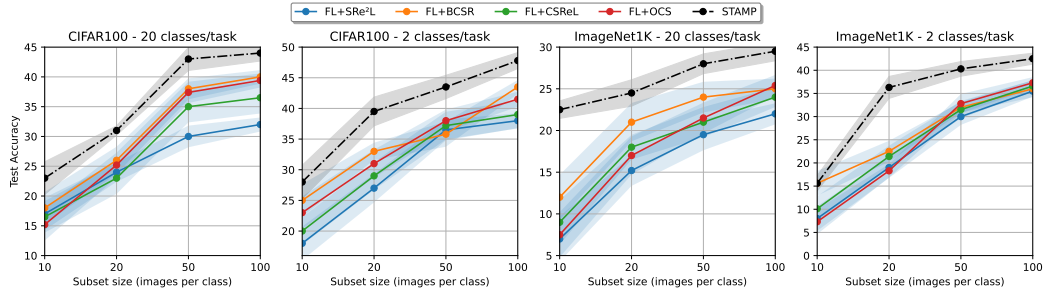


Figure 4: Performance comparisons in coreset selection demonstrate that our approach outperforms the integration of alternative baseline methods within vanilla FL.

4.3.2 Efficiency of Temporal Gradient Matching

To evaluate the effectiveness of temporal gradient matching on the client side, we analyze the gradient angles produced by STAMP on CIFAR100 and ImageNet1K datasets and compare them with two sets of baseline methods: FedAvg and FedL2P for standard FL, and FedWeIT and AF-FCL, for FCL. The results are presented in Figure 5. As shown, STAMP demonstrates superior gradient alignment with previously learned tasks. This improved alignment suggests that STAMP is less prone to catastrophic forgetting compared to existing approaches.

4.3.3 Efficiency of Spatio Gradient Matching

Figure 6 presents the gradient divergence across various baseline methods on CIFAR100 and ImageNet1K, evaluated under two different settings: 20 classes per task and the more challenging 2 classes per task. It is evident that, unlike existing baselines which generally overlook the alignment among client gradients, STAMP achieves significantly better gradient alignment. This improved alignment facilitates model updates that more effectively seek invariant aggregated gradient directions across clients for specific tasks, thereby enhancing the generalization capability of the aggregated model. This observation is consistent with the reduced global-local generalization gap demonstrated in Figure 1b.

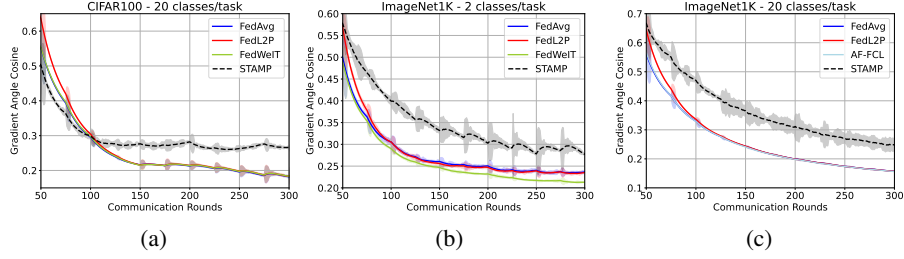


Figure 5: The figures illustrate the average temporal gradient angles across different baseline methods. Specifically, Figure 5a shows the gradient cosine similarity on CIFAR100 under a 20 classes per task setting. Figure 5b presents the gradient cosine similarity for ImageNet1K with 2 classes per task, and Figure 5c depicts the results for ImageNet1K under a 20 classes per task configuration.

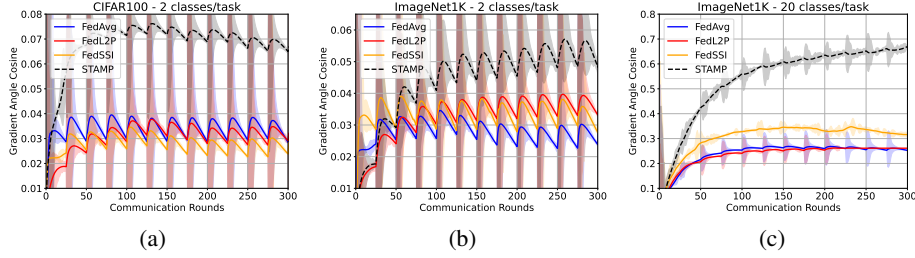


Figure 6: The figures illustrate the average spatio gradient angles across different baseline methods. Specifically, Figure 6a shows the gradient cosine similarity on CIFAR100 under a 2 classes per task setting. Similarly, Figure 6b presents the gradient cosine similarity for ImageNet1K with 2 classes per task, and Figure 6c depicts the results for ImageNet1K under a 20 classes per task configuration.

4.4 Ablation Study on STAMP

Table 3 presents the ablation results for each component. The results demonstrate that both Spatio grAdient Matching (SAM) and Temporal grAdient Matching (TAM) consistently enhance the average classification accuracy. Notably, SAM contributes more significantly to accuracy improvement by enhancing generalization across tasks within a single communication round. In contrast, TAM plays a more critical role in reducing average forgetting by mitigating catastrophic forgetting; it achieves this by aligning the learned gradients with those from previous tasks on the same client. Additionally, the use of the prototypical coreset selection method further boosts the performance of STAMP by improving data representation through ProtoNet.

Table 3: We conduct ablation studies on the CIFAR100 and ImageNet1K datasets, using 10 clients and 2 classes per task. Specifically, (1) refers to spatio-temporal gradient matching performed on the server side, (2) denotes temporal gradient matching executed on the client side, and (3) corresponds to the use of a prototypical coreset implemented with ProtoNet.

Dataset	Metric	FedAvg	(1)	(2)	(1) + (2)	(1) + (3)	(2) + (3)	STAMP
CIFAR100	Acc.	31.7 (± 1.7)	38.1 (± 1.3)	37.8 (± 0.6)	44.7 (± 1.5)	46.1 (± 0.7)	44.9 (± 1.4)	52.8 (± 0.9)
	AF	22.1 (± 1.3)	23.8 (± 0.4)	21.7 (± 0.9)	21.5 (± 1.0)	24.7 (± 1.4)	21.8 (± 0.6)	24.3 (± 0.8)
ImageNet1K	Acc.	24.3 (± 5.1)	30.5 (± 2.8)	28.3 (± 2.6)	34.1 (± 0.7)	37.4 (± 1.1)	36.5 (± 1.3)	41.5 (± 2.8)
	AF	19.6 (± 0.1)	26.1 (± 0.7)	23.8 (± 0.6)	24.3 (± 0.9)	26.1 (± 1.8)	23.3 (± 0.8)	24.2 (± 0.8)

5 Conclusion

In this paper, we have tackled the challenges of FCL in realistic settings characterized by client data heterogeneity and task conflicts. Recognizing the limitations of existing generative replay-based methods, we have introduced a novel model-agnostic approach, Spatio-Temporal Gradient Matching with Network-Free Prototype Coreset. Our method effectively mitigates catastrophic forgetting and data bias by leveraging prototype samples for robust gradient approximation and applying gradient matching both temporally and spatially. Through extensive experiments, we have demonstrated that our approach consistently outperforms existing baselines, highlighting its potential as a powerful solution for resilient FCL in diverse, dynamic environments.

References

- Balunovic, M., Dimitrov, D. I., Staab, R., and Vechev, M. Bayesian framework for gradient leakage. In *Int. Conf. Learn. Represent.*, May 2022.
- Chen, J., Cong, R., LUO, Y., Ip, H., and Kwong, S. Saving 100x storage: Prototype replay for reconstructing training sample distribution in class-incremental semantic segmentation. In *Adv. Neural Inform. Process. Syst.*, Dec. 2023.
- Deng, D., Chen, G., Hao, J., Wang, Q., and Heng, P.-A. Flattening sharpness for dynamic gradient projection memory benefits continual learning. In *Adv. Neural Inform. Process. Syst.*, Dec. 2021.
- Deng, J., Dong, W., Socher, R., Li, L.-J., Li, K., and Fei-Fei, L. Imagenet: A large-scale hierarchical image database. In *IEEE Conf. Comput. Vis. Pattern Recog.*, Aug. 2009.
- Dimitrov, D. I., Balunovic, M., Konstantinov, N., and Vechev, M. Data leakage in federated averaging. *Transactions on Machine Learning Research*, Nov. 2022.
- Dohare, S., Hernandez-Garcia, J. F., Lan, Q., et al. Loss of plasticity in deep continual learning. *Nature*, Aug. 2024.
- Dong, J., Wang, L., Fang, Z., Sun, G., Xu, S., Wang, X., and Zhu, Q. Federated class-incremental learning. In *IEEE Conf. Comput. Vis. Pattern Recog.*, Apr. 2022.
- Dong, J., Zhang, D., Cong, Y., Cong, W., Ding, H., and Dai, D. Federated incremental semantic segmentation. In *IEEE Conf. Comput. Vis. Pattern Recog.*, pp. 3934–3943, Jun. 2023.
- Dong, J., Li, H., Cong, Y., Sun, G., Zhang, Y., and Van Gool, L. No One Left Behind: Real-World Federated Class-Incremental Learning. *IEEE Patt. Ana. and Mach. Intell.*, 46(04):2054–2070, Apr. 2024. ISSN 1939-3539.
- Elsayed, M. and Mahmood, A. R. Addressing loss of plasticity and catastrophic forgetting in continual learning. In *Int. Conf. Learn. Represent.*, May 2024.
- Fantauzzo, L., Fanì, E., Caldarola, D., Tavera, A., Cermelli, F., Ciccone, M., and Caputo, B. FedDrive: Generalizing federated learning to semantic segmentation in autonomous driving. Oct. 2022.
- Goswami, D., Liu, Y., Twardowski, B., and van de Weijer, J. FeCAM: Exploiting the heterogeneity of class distributions in exemplar-free continual learning. In *Adv. Neural Inform. Process. Syst.*, Dec. 2023.
- Hao, J., Ji, K., and Liu, M. Bilevel coreset selection in continual learning: A new formulation and algorithm. In *Adv. Neural Inform. Process. Syst.*, Dec. 2023.
- He, K., Zhang, X., Ren, S., and Sun, J. Deep residual learning for image recognition. In *Proceedings of the IEEE Conference on Computer Vision and Pattern Recognition (CVPR)*, pp. 770–778, 2016.
- Krizhevsky, A. Learning multiple layers of features from tiny images. Technical report, University of Toronto, 2009. Technical Report.
- Lee, R., Kim, M., Li, D., Qiu, X., Hospedales, T., Huszár, F., and Lane, N. D. Fedl2p: Federated learning to personalize. In *Adv. Neural Inform. Process. Syst.*, Dec. 2023.
- Li, D., Zhang, A., Gao, J., and Qi, B. An efficient memory module for graph few-shot class-incremental learning. In *Adv. Neural Inform. Process. Syst.*, Dec. 2024a.
- Li, Y., Li, Q., Wang, H., Li, R., Zhong, W., and Zhang, G. Towards efficient replay in federated incremental learning. In *Proceedings of the IEEE/CVF Conference on Computer Vision and Pattern Recognition (CVPR)*, pp. 12820–12829, Jun. 2024b.
- Li, Y., Xu, W., Qi, Y., Wang, H., Li, R., and Guo, S. SR-FDIL: Synergistic replay for federated domain-incremental learning. *IEEE Transactions on Parallel and Distributed Systems*, 35(11): 1879–1890, 2024c.
- Li, Y., Wang, Y., Xiao, T., Wang, H., Qi, Y., and Li, R. FedSSI: Rehearsal-free continual federated learning with synergistic synaptic intelligence. In *Int. Conf. Mach. Learn.*, Jul. 2025a.

- Li, Y., Xu, W., Wang, H., Qi, Y., Guo, J., and Li, R. Personalized federated domain-incremental learning based on adaptive knowledge matching. In *Eur. Conf. Comput. Vis.*, Apr. 2025b.
- Lim, W. Y. B., Luong, N. C., Hoang, D. T., Jiao, Y., Liang, Y.-C., Yang, Q., Niyato, D., and Miao, C. Federated learning in mobile edge networks: A comprehensive survey. *IEEE Comm. Surveys & Tutorials*, Jun. 2020.
- Liu, Z., Lin, Y., Cao, Y., Hu, H., Wei, Y., Zhang, Z., Lin, S., and Guo, B. Swin transformer: Hierarchical vision transformer using shifted windows. In *Proceedings of the IEEE/CVF International Conference on Computer Vision (ICCV)*, pp. 10012–10022, 2021.
- Lopez-Paz, D. and Ranzato, M. A. Gradient episodic memory for continual learning. In Guyon, I., Luxburg, U. V., Bengio, S., Wallach, H., Fergus, R., Vishwanathan, S., and Garnett, R. (eds.), *Adv. Neural Inform. Process. Syst.*, Dec. 2017.
- Luo, K., Li, X., Lan, Y., and Gao, M. Gradma: A gradient-memory-based accelerated federated learning with alleviated catastrophic forgetting. In *IEEE Conf. Comput. Vis. Pattern Recog.*, pp. 3708–3717, Jun. 2023.
- McMahan, B., Moore, E., Ramage, D., Hampson, S., and Arcas, B. A. y. Communication-Efficient Learning of Deep Networks from Decentralized Data. In *Int. Conf. on AISTATS*, Apr. 2017.
- Mirzadeh, S.-I., Farajtabar, M., Görür, D., Pascanu, R., and Ghasemzadeh, H. Linear mode connectivity in multitask and continual learning. In *Proceedings of the 9th International Conference on Learning Representations (ICLR)*, 2021.
- Nguyen, D. C., Pham, Q.-V., Pathirana, P. N., Ding, M., Seneviratne, A., Lin, Z., Dobre, O., and Hwang, W.-J. Federated learning for smart healthcare: A survey. *ACM Comput. Surv.*, 55, Mar. 2023a.
- Nguyen, M.-D., Lee, S.-M., Pham, Q.-V., Hoang, D. T., Nguyen, D. N., and Hwang, W.-J. HCFL: A high compression approach for communication-efficient federated learning in very large scale IoT networks. *IEEE Trans. on Mob. Comp.*, Jul. 2023b.
- Nguyen, T.-B., Nguyen, M.-D., Park, J., Pham, Q.-V., and Hwang, W. J. Federated domain generalization with data-free on-server gradient matching. In *Int. Conf. Learn. Represent.*, May 2025.
- Nguyen, T. D., Nguyen, T. A., Tran, A., Doan, K. D., and Wong, K.-S. IBA: Towards irreversible backdoor attacks in federated learning. In *Adv. Neural Inform. Process. Syst.*, Dec. 2023c.
- Petrov, I., Dimitrov, D. I., Baader, M., Müller, M. N., and Vechev, M. DAGER: Exact gradient inversion for large language models. In *Adv. Neural Inform. Process. Syst.*, Dec. 2024.
- Qi, D., Zhao, H., and Li, S. Better generative replay for continual federated learning. In *Int. Conf. Learn. Represent.*, May 2023.
- Saha, G., Garg, I., and Roy, K. Gradient projection memory for continual learning. In *Int. Conf. Learn. Represent.*, May 2021.
- Snell, J., Swersky, K., and Zemel, R. Prototypical networks for few-shot learning. In *Adv. Neural Inform. Process. Syst.*, Dec. 2017.
- Tong, R., Liu, Y., Shi, J. Q., and Gong, D. Coreset selection via reducible loss in continual learning. In *Int. Conf. Learn. Represent.*, Dec. 2025.
- Tran, M.-T., Le, T., Le, X.-M., Harandi, M., and Phung, D. Text-enhanced data-free approach for federated class-incremental learning. In *IEEE Conf. Comput. Vis. Pattern Recog.*, Jun. 2024.
- Wan, Y., Qu, Y., Ni, W., Xiang, Y., Gao, L., and Hossain, E. Data and model poisoning backdoor attacks on wireless federated learning, and the defense mechanisms: A comprehensive survey. *IEEE Comm. Surveys & Tutorials*, Feb. 2024.
- Wang, Q., Liu, B., and Li, Y. Traceable federated continual learning. In *IEEE Conf. Comput. Vis. Pattern Recog.*, Jul. 2024.

- Wei, Y., Ye, J., Huang, Z., Zhang, J., and Shan, H. Online Prototype Learning for Online Continual Learning. In *Int. Conf. Comput. Vis.*, Oct. 2023.
- Wu, Y., Huang, L.-K., Wang, R., Meng, D., and Wei, Y. Meta continual learning revisited: Implicitly enhancing online hessian approximation via variance reduction. In *Int. Conf. Learn. Represent.*, Dec. 2024.
- Wuerkaixi, A., Cui, S., Zhang, J., Yan, K., Han, B., Niu, G., Fang, L., Zhang, C., and Sugiyama, M. Accurate forgetting for heterogeneous federated continual learning. In *Int. Conf. Learn. Represent.*, May 2024.
- Yang, E., Shen, L., Wang, Z., Liu, S., Guo, G., and Wang, X. Data augmented flatness-aware gradient projection for continual learning. In *Int. Conf. Comput. Vis.*, pp. 5630–5639, Oct. 2023.
- Yang, X., Huang, W., and Ye, M. Fedas: Bridging inconsistency in personalized federated learning. In *IEEE Conf. Comput. Vis. Pattern Recog.*, Jun. 2024.
- Yin, Z., Xing, E., and Shen, Z. Squeeze, recover and relabel: Dataset condensation at imagenet scale from a new perspective. In *Adv. Neural Inform. Process. Syst.*, Dec. 2023.
- Yoon, J., Jeong, W., Lee, G., Yang, E., and Hwang, S. J. Federated continual learning with weighted inter-client transfer. In *Int. Conf. Mach. Learn.*, Jul. 2021.
- Yoon, J., Madaan, D., Yang, E., and Hwang, S. J. Online coreset selection for rehearsal-based continual learning. In *Int. Conf. Learn. Represent.*, May 2022.
- Zhang, J., Chen, C., Zhuang, W., and Lyu, L. TARGET: Federated Class-Continual Learning via Exemplar-Free Distillation . In *Int. Conf. Comput. Vis.*, Oct. 2023a.
- Zhang, J., Hua, Y., Cao, J., Wang, H., Song, T., Xue, Z., Ma, R., and Guan, H. Eliminating domain bias for federated learning in representation space. In *Adv. Neural Inform. Process. Syst.*, Dec. 2023b.
- Zhang, J., Hua, Y., Wang, H., Song, T., Xue, Z., Ma, R., and Guan, H. Fedala: Adaptive local aggregation for personalized federated learning. In *AAAI*, volume 37, Jun. 2023c.
- Zhang, J., Liu, Y., Hua, Y., Wang, H., Song, T., Xue, Z., Ma, R., and Cao, J. PFLlib: A beginner-friendly and comprehensive personalized federated learning library and benchmark. *Journal of Machine Learning Research*, Feb. 2025.
- Zhen, X., Du, Y., Xiong, H., Qiu, Q., Snoek, C., and Shao, L. Learning to learn variational semantic memory. In *Adv. Neural Inform. Process. Syst.*, Dec. 2020.
- Zhou, K., Yang, Y., Qiao, Y., and Xiang, T. Domain generalization with mixstyle. In *Int. Conf. Learn. Represent.*, May 2021.

A Detailed Algorithms

Algorithm 1: Pseudo Algorithm of STAMP. The **box** refers to the **S**patio **g**radient **M**atching (SAM), the **box** refers to the **T**emporal **g**radient **M**atching (TAM), the **box** refers to the **p**rototypical **c**oreset **s**election (PCS).

Input: set of source clients \mathcal{U}_S , number of communication rounds R , local learning rate η , global learning rate η_g , searching space hyper-parameter κ .

Output: $\theta_g^{(R)}$

```

1 Clients Update:
2 for client  $u \in \mathcal{U}_S$  do
3   Receive global model  $\theta_u^{(r)} = \theta_g^{(r)}$ ;
4   Compute  $p^l = \frac{1}{\sum_{t=1}^T |\mathcal{N}_l^t|} \left[ g(\tilde{x}^l; \phi) \cdot \sum_{j=1}^{t-1} |\mathcal{N}_l^j| + \sum_{i \in \mathcal{N}_l^t} g(x_i; \phi) \right] \cdot \mathbb{1}\{y_j = l\}$ ,
5   Initialize learnable coefficient set  $A = \{a_i | i \in \mathcal{N}_l^t\}$ 
6   Solve  $\tilde{X}^l = \arg \min_A \left\| \left[ \frac{1}{|\mathcal{M}^l|} \sum_{i \in \mathcal{M}^l} g(x_i; \phi) + \frac{1}{|\mathcal{N}_l^t|} \sum_{i \in \mathcal{N}_l^t} a_i \cdot g(x_i; \phi) \right] - p^l \right\|^2$ ,
7    $\tilde{x}^l = \text{MixStyle}(\tilde{x}^l; x)$ ,
8   Save new proto into replay memory  $\mathcal{M}^t = \tilde{x}^l$ .
9   for local epoch  $e \in E$  do
10    Sample mini-batch  $\zeta$  from local data  $\mathcal{D}_u$ ;
11    Calculate gradient  $g_u^{t,r,e} = \nabla \mathcal{E}(\theta_u^{(r,e)}, \zeta)$ ;
12  end for
13  Calculate  $\tilde{g}^t = \frac{1}{E} \sum_{e=1}^E g_u^{t,r,e}$ .
14  for task  $i = 1, \dots, t-1$  do
15    Sample coreset  $\zeta$  from replay memory  $\mathcal{M}^i$  according to task  $i$ ,
16    Calculate task-wise gradients:  $\tilde{g}_u^i = \nabla \mathcal{E}(\theta_u^{(r,e)}, \zeta)$ .
17  end for
18   $\mathbf{g} = [\tilde{g}_u^1, \dots, \tilde{g}_u^t]$ , and  $\bar{g} = \sum_{i=1}^t g_u^i$ ,
19  Solve:  $\Gamma^* = \arg \min_{\Gamma} \Gamma \mathbf{g} \cdot \bar{g} + \kappa \|\bar{g}\| \|\Gamma \mathbf{g}^{(t,r)}\|$ ,
20  Update TAM:  $g_{\text{TAM}} = \bar{g} + \frac{\kappa \|\bar{g}\|}{\|\Gamma^* \mathbf{g}^{(t,r)}\|} \Gamma^* \mathbf{g}^{(t,r)}$ ,
21  Model steps with aggregated gradient:  $\theta_u^{(t,r)} = \theta_u^{(t,r-1)} - \eta_g g_{\text{TAM}}^{(t,r)}$ .
22  Upload client's model  $\theta_u^{(t,r+1)}$  to server;
23 end for
24 Server Optimization:
25 for task  $t = 0, \dots$  do
26   for round  $r = 0, \dots, R$  do
27     Clients Updates;
28     Calculate  $g_u^{(t,r)} = \theta_u^{(t,r+1)} - \theta_u^{(t,r)}$ ,  $\mathbf{g}^{(t,r)} = \{g_u^{(t,r)} | u \in \mathcal{U}_S\}$ ;
29     Calculate  $g_{\text{FL}}^{(t,r)}$  (e.g.,  $g_{\text{FL}}^{(t,r)} = \frac{1}{U} \sum_{u=1}^U g_u^{(t,r)}$  as the FedAvg update);
30     Solve:  $\Gamma^* = \arg \min_{\Gamma} \Gamma \mathbf{g}^{(t,r)} \cdot g_{\text{FL}}^{(t,r)} + \kappa \|g_{\text{FL}}^{(t,r)}\| \|\Gamma \mathbf{g}^{(t,r)}\|$ ,
31     Update SAM:  $g_{\text{SAM}}^{(t,r)} = g_{\text{FL}}^{(t,r)} + \frac{\kappa \|g_{\text{FL}}^{(t,r)}\|}{\|\Gamma^* \mathbf{g}^{(t,r)}\|} \Gamma^* \mathbf{g}^{(t,r)}$ ,
32     Model steps with aggregated gradient:  $\theta_u^{(t,r+1)} = \theta_u^{(t,r)} - \eta_u g_{\text{SAM}}^{(t,r)}$ .
33   end for
34 end for

```

B Related Works

B.1 Importance-based Sampling

LGA (Dong et al., 2024) introduces a method to balance the contributions of different classes to the gradient, aiming to mitigate catastrophic forgetting caused by imbalance among incremental tasks. Re-Fed (Li et al., 2024b) presents a method for quantifying an importance score, which is utilized to selectively retain cached samples within the replay memory. FedWeIT (Yoon et al., 2021) partitions network weights into global federated and sparse task-specific parameters, enabling clients to selectively acquire knowledge through a weighted combination of others’ task-specific parameters. FedSSI (Li et al., 2025a) introduces a regularization technique that estimates the importance of each synaptic weight change during training. It penalizes substantial changes to weights deemed important for previously learned tasks, thereby helping to preserve prior knowledge.

B.2 Prototype-based Learning

SR-FDIL (Li et al., 2024c) introduces an approach that utilizes data from the local replay memory to train both the prototype generator and the discriminator on local devices. TagFed (Wang et al., 2024) proposes a method to identify repetitive data features from previous tasks and augment them for the current task prior to federation, thereby enhancing overall performance.

B.3 Gradient Memory

GradMA (Luo et al., 2023) employs gradient projection on the client side, correcting gradients via quadrature optimization using stored gradients from other clients.

B.4 Generative Replay Memory

FedCIL (Qi et al., 2023) introduces an efficient approach for training GAN-based replay memory in distributed systems. TARGET (Zhang et al., 2023a) introduces an approach that learns a server-side generative model capable of producing data that adheres to the global model distribution. This generated data is subsequently used to update the client-side student model via knowledge distillation. AF-FCL (Wuerkaixi et al., 2024) introduces a generative model that employs a learned normalizing flow to capture and retain the essential data distribution while effectively eliminating biased features. pFedDIL (Li et al., 2025b) proposes an approach that transfers knowledge across incremental tasks by using a small auxiliary classifier in each personalized model to distinguish its specific task from others. FBL (Dong et al., 2023) uses adaptive class-balanced pseudo labeling along with semantic compensation and relation consistency losses to generate reliable pseudo labels and balance gradient propagation, thereby mitigating the effects of background shifts.

B.5 Episodic Replay Memory for Continual Learning

GEM (Lopez-Paz & Ranzato, 2017) introduced an episodic memory mechanism that stores a subset of data samples, enabling the estimation of task-specific gradients. This approach facilitates gradient projection, thereby mitigating catastrophic forgetting in CL. VR-MCL (Wu et al., 2024) introduced a meta CL approach that effectively utilizes data stored in the memory buffer.

Authors in (Qi et al., 2023) demonstrate that incorporating a GAN-based replay memory in a distributed system can be significantly affected by feature shifts among clients. To address this challenge, FedCIL introduces a distillation-based approach designed to mitigate discrepancies across different domains. GPM (Saha et al., 2021) introduces a method for storing gradient projections in replay memory as an alternative to retaining previous data, thereby facilitating CL. FS-DGPM (Deng et al., 2021) introduces an enhanced version of GPM, in which the projected gradients are flattened. This flattening process improves generalization and enhances robustness to noise caused by a sharp loss landscape.

C Experimental Details

We utilize the pFLlib framework (Zhang et al., 2025) as FL core framework to design the FCL settings. All experiments are conducted using four NVIDIA GeForce RTX 4090 GPUs and two NVIDIA GeForce RTX 3090 GPUs. The detailed experimental configurations are outlined below:

C.1 Datasets

C.1.1 Heterogeneous Federated Continual Learning Settings

Our work investigates the behavior of various algorithms in a heterogeneous FCL setting. To align with a realistic and challenging non-IID federated scenario, we increase the difficulty by adopting the task design proposed by (Dohare et al., 2024), in which we construct a sequence of classification tasks by taking the classes in groups.

Example 1 *For example, in case of binary classification, one task could involve differentiating chickens from llamas, while another might focus on differentiating phones from computers.*

To consider the performance of baselines under different level of heterogeneity, we consider two experimental scenarios. In the first, each task comprises 20 distinct classes. This setup represents the conventional task configuration commonly used in existing literature (Wuerkaixi et al., 2024). In the second, each task contains only 2 classes, creating a more challenging environment. In this case, models are more likely to overfit to individual tasks, making them more susceptible to catastrophic forgetting when adapting to new tasks. Simultaneously, client divergence becomes more pronounced under this configuration.

Specifically, we utilize two widely adopted benchmark datasets:

Non-Overlapped-CIFAR100. The CIFAR100 dataset (Krizhevsky, 2009) consists of 100 object categories, with a total of 60,000 images. Each image has a resolution of 32×32 pixels. In case 1 task comprises 2 classes, we can form 4950 distinct tasks. In case 1 task comprises 20 classes, we can form more than 5×10^{20} distinct tasks.

Non-Overlapped-ImageNet1K. ImageNet1K dataset (Deng et al., 2009) contains 1,000 diverse object categories, with over 1.3 million high-resolution training images. All images are resized to 224×224 pixels during preprocessing. In case 1 task comprises 2 classes, we can form half a million tasks. In case 1 task comprises 20 classes, we can form more than 3×10^{41} distinct tasks. The scale and diversity of ImageNet1K pose greater challenges in terms of memory footprint, computational cost, and model scalability.

C.2 Baselines

We evaluate our approach against several established baselines from FL, and FCL. For conventional FL baselines, we compare with standard methods such as FedAvg (McMahan et al., 2017), FedALA (Zhang et al., 2023c), FedDBE (Zhang et al., 2023b), FedL2P (Lee et al., 2023), and FedAS (Yang et al., 2024), FedOMG (Nguyen et al., 2025). FedAvg serves as the foundational baseline in FL. FedALA, FedL2P, and FedAS focus on personalized FL, enabling models to adapt to client-specific tasks and thereby mitigating the effects of task heterogeneity. In contrast, FedDBE and FedOMG aim to construct a more robust global model by reducing inter-client bias, thereby enhancing generalization across both tasks and clients.

For FCL, we assess several state-of-the-arts, including FedWeIT (Yoon et al., 2021), GLFC (Dong et al., 2022), FedCIL (Qi et al., 2023), LANDER (Tran et al., 2024), TARGET (Zhang et al., 2023a), FedSSI (Li et al., 2025a), and AF-FCL (Wuerkaixi et al., 2024). FedWeIT exemplifies approaches that allocate specialized expert modules for each task, allowing task-specific adaptation. GLFC uses a distillation-based approach to address catastrophic forgetting, considering both local and global aspects. FedCIL, LANDER, TARGET, and AF-FCL adopt generative replay strategies, training generative models on each client to synthesize pseudo-data for previously encountered tasks. Among these, AF-FCL is the most recent and directly addresses the challenges posed by heterogeneous FCL settings, making it a particularly relevant benchmark for comparison.

C.3 Evaluation Metrics

To evaluate the baselines, we utilize two standard metrics from the CL literature (Yoon et al., 2021), (Mirzadeh et al., 2021), which are well-suited for tracking the performance of a global model in FL, coined accuracy and averaged forgetting.

Averaged Forgetting. This metric measures the decline from a task’s highest accuracy, which is typically achieved right after it is trained, to its final accuracy after all tasks have been learned. For T tasks, the forgetting is defined as

$$AF = \frac{1}{T-1} \sum_{i=1}^{T-1} \max_{t \in \{1, \dots, T-1\}} (a_{t,i} - a_{T,i}). \quad (9)$$

As the model shifts focus to new tasks, its performance on earlier ones often decreases. Therefore, minimizing forgetting is important to maintain overall performance.

C.4 Architecture Details

For CIFAR-10, CIFAR100, Digit10, and Office31, we adopt conventional ResNet-18 (He et al., 2016) as the backbone network architecture for all validation experiments. For ImageNet1K, we employ Swin Transformer Tiny (Swin-T) (Liu et al., 2021) as the backbone. It is noted that FCIL, LANDER, TARGET, FedL2P, FedWeIT and AF-FCL use addition generative networks or modify their network architectures, with details summarized in the following table. We denote FedWeIT (T) as the version theoretically proposed in the original paper, while FedWeIT (C) represents the configuration observed in our experimental implementation.

Table 4: Architectural details of methods with modified models.

Method	CIFAR-10, CIFAR100, Digit10, Office31		ImageNet1K	
	Model	#Params	Model	#Params
FedAvg	ResNet-18	11.7 M	Swin-T	28.8 M
FedSSI	ResNet-18	11.7 M	Swin-T	28.8 M
FCIL	ResNet-18 + GAN	16.1 M	Swin-T + GAN	49.7 M
LANDER	ResNet-18 + GAN	16.1 M	Swin-T + GAN	49.7 M
TARGET	ResNet-18 + GAN	16.1 M	Swin-T + GAN	49.7 M
FedL2P	ResNet-18 + Meta-Net	13.5 M	Swin-T + Meta-Net	32.6 M
FedWeIT (T)	Modified ResNet-18	596.2 M	Modified Swin-T	7192.3 M
FedWeIT (C)	Modified LeNet	171.8 B		
AF-FCL	ResNet-18 + NFlow	21.3 M	Swin-T + NFlow	53.4 M

Specifically, FedWeIT augments the base model with sparse task-adaptive parameters, task-specific masks over local base parameters, and attention weights for inter-client knowledge transfer. FCIL, LANDER, and TARGET incorporate additional GANs to learn past task features. FedL2P introduces a meta-net that generates personalized hyper-parameters, such as batch normalization statistics and learning rates, adapted to each client’s local data distribution to improve learning on non-IID data. AF-FCL additionally requires a normalizing flow generative model (NFlow¹) for credibility estimation and generative replay mechanism, which guide selective retention and forgetting.

C.5 Training Details

In our proposed heterogeneous federated continual learning framework for the CIFAR100 and ImageNet1K datasets, we consider a setting involving 10 clients with a client participation fraction of 1.0. We do not adopt a conventional non-IID distribution in this scenario; instead, each client is assigned distinct classes, which introduces a level of heterogeneity that is more challenging than typical non-IID configurations.

¹NFlow refers to the normalizing flow model, where the example is provided in <https://github.com/zaocan666/AF-FCL/blob/main/FLAlgorithms/PreciseFCLNet/model.py>

Additionally, we evaluate the proposed approach under non-IID conditions using four benchmark datasets: CIFAR-10, CIFAR100, Digit-10, and Office-31. For these experiments, we simulate data heterogeneity using the Dirichlet distribution with varying concentration parameters (e.g., $\alpha = 0.1, 1.0, 10.0$, and 100.0) to control the degree of non-IID-ness. The complete details of the experimental settings are provided in Table 5.

Table 5: Experimental Details. Settings for heterogeneous and non-IID distributed FCL.

Attributes	Heterogeneous FCL		Non-IID distributed FCL			
	CIFAR100	ImageNet1K	CIFAR10	CIFAR100	Digit10	Office31
Task size	141 MB / 14 MB	8 GB / 0.8 GB	141 MB	141 MB	480 M	88 M
Image number	60K	1.3M	60K	60K	110K	4.6K
Image Size	$3 \times 32 \times 32$	$3 \times 224 \times 224$	$3 \times 32 \times 32$	$3 \times 32 \times 32$	$1 \times 28 \times 28$	$3 \times 300 \times 300$
Task number	5 / 50	50 / 500	5	10	4	3
Batch Size	128	128	64	64	64	32
Learning Rate	0.005	0.005	0.01	0.01	0.001	0.01
Data heterogeneity	N/A	N/A	0.1	10.0	0.1	1.0
Client numbers	10	10	10	10	10	10
Local training epoch	5	5	5	5	5	5
Client selection ratio	1.0	1.0	1.0	1.0	1.0	1.0
Rounds per Task	25	25	80	100	60	60

D Additional Experimental Evaluations

D.1 Experimental Evaluations on Pretrained Models

Figure 7 illustrates the performance of FedAvg and STAMP on the ImageNet1K dataset using a pretrained model. Given that the model is pretrained on the same dataset, the evaluation may suffer from overfitting. Consequently, the experimental results show no substantial performance difference between the two algorithms. Moreover, the issue of catastrophic forgetting appears to be minimal in this evaluation setting.

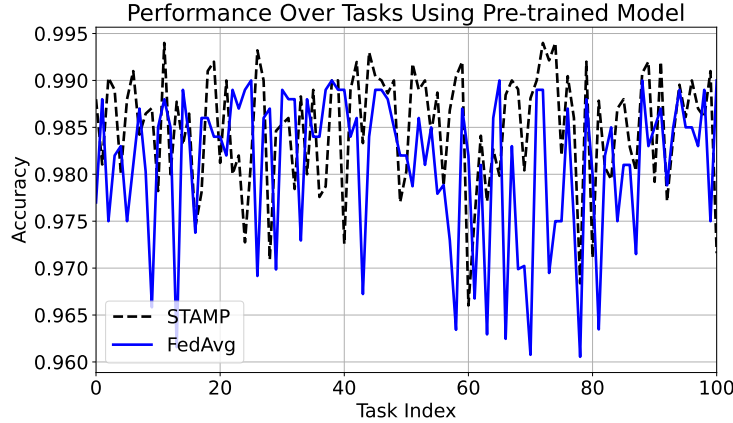


Figure 7: Accuracy on ImageNet1K with Pretrained Models.

D.2 Hyper-parameter tuning for STAMP

In this section, we examine the impact of various hyperparameters through a series of experiments conducted on the ImageNet-1K dataset. For each experiment, one specific hyperparameter is varied while all other hyperparameters are held constant.

D.2.1 Gradient Normalization

Since STAMP is sensitive to the magnitude of local gradients, the presence of a dominant subset with disproportionately large gradient magnitudes can bias the optimization process toward that subset during gradient matching. Figure 8 illustrates the impact of applying gradient normalization on both the client and server sides before performing gradient matching. With gradient normalization in place, STAMP demonstrates a notable improvement in performance.

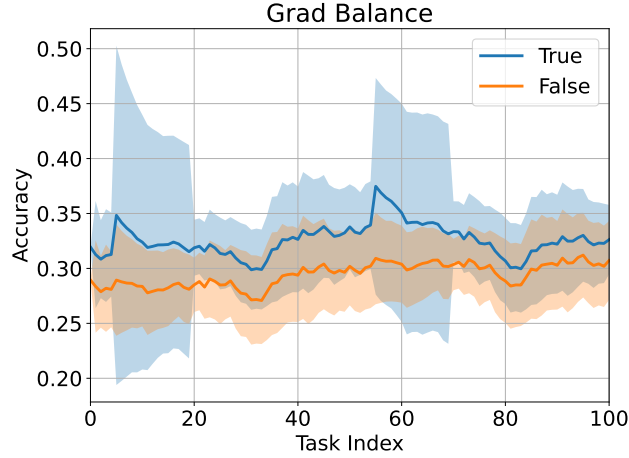


Figure 8: Analysis on Gradient Normalization.

D.2.2 Local Epoch

Selecting the number of local epochs is crucial, as increasing the number of local epochs leads to a more accurate approximation of the local gradient trajectory. Figure 9 illustrates the performance of STAMP under varying numbers of local epochs.

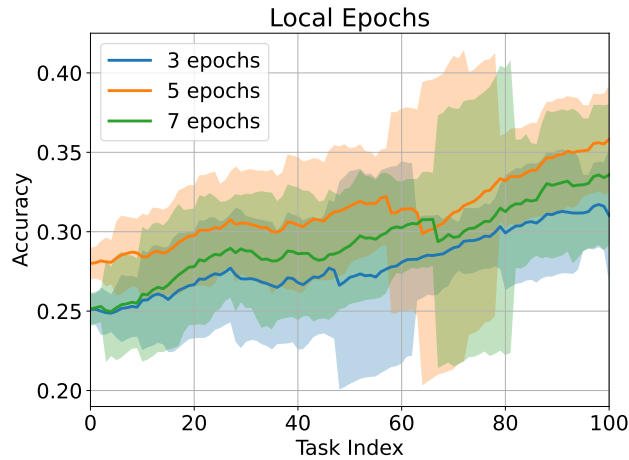


Figure 9: Analysis on different number of local epochs.

D.2.3 Local Learning Rate

Figure 10 illustrates the performance of STAMP under different local learning rate.

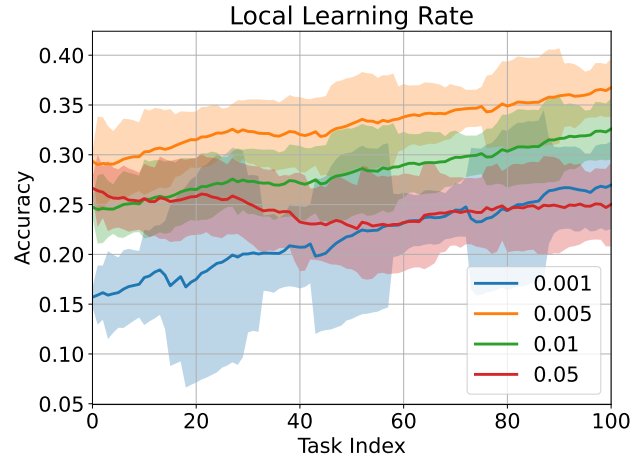


Figure 10: Analysis on different local learning rate.

D.2.4 Gradient Matching Searching Radius

Figure 11 illustrates the impact of the search radius on gradient matching in STAMP. Selecting an appropriate search radius (e.g., 0.5) is critical for achieving an optimal gradient matching solution. A smaller radius (e.g., 0.1) constrains the search space too tightly, causing the solution to converge toward the average gradient and reducing matching effectiveness. Conversely, a larger radius (e.g., 0.75) broadens the search space excessively, making it difficult to identify an optimal solution.

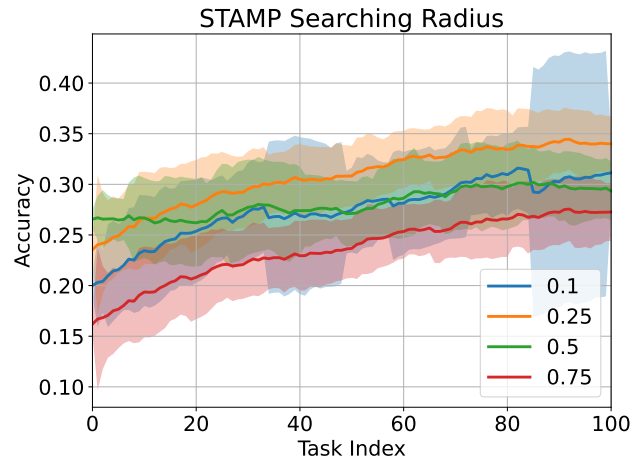


Figure 11: Analysis on different searching radius.

D.2.5 Gradient Matching Step Size & Momentum

Figures 12 and 13 demonstrate the effects of momentum and learning rate scheduling on gradient matching performance.

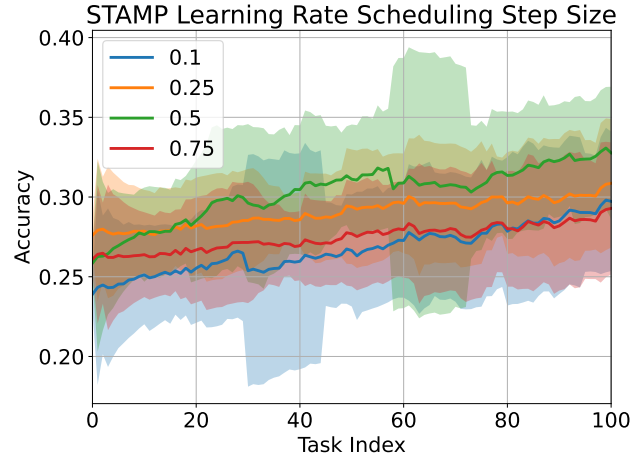


Figure 12: Analysis on different learning rate scheduling step size.

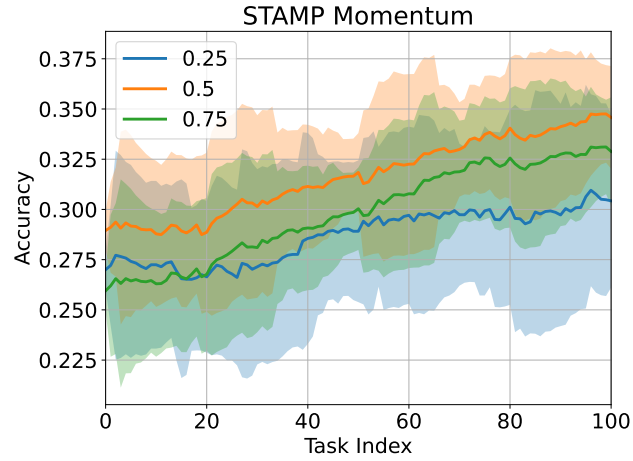


Figure 13: Analysis on different momentum for gradient matching.

D.2.6 Gradient Matching Number of Rounds

Figure 14 illustrates the impact of the number of optimization steps on the efficiency of gradient matching.

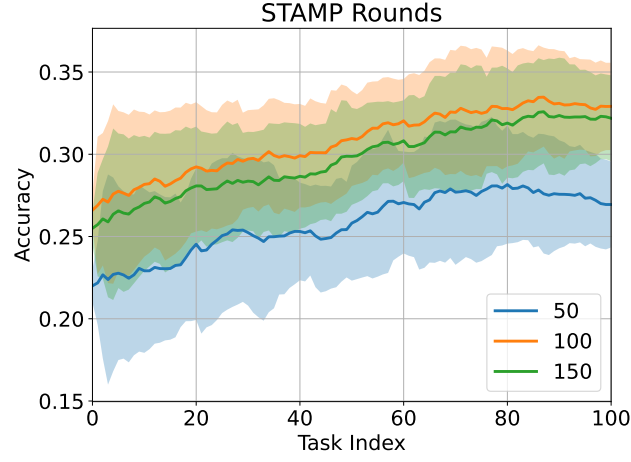


Figure 14: Analysis on different number of rounds

D.2.7 Gradient Matching Scheduling Step Size

Figure 15 illustrates the performance of STAMP under various learning rate scheduler step sizes. Selecting an appropriate step size (e.g., 30) facilitates optimal gradient matching decisions, thereby enhancing the stability and efficiency of FCL training.

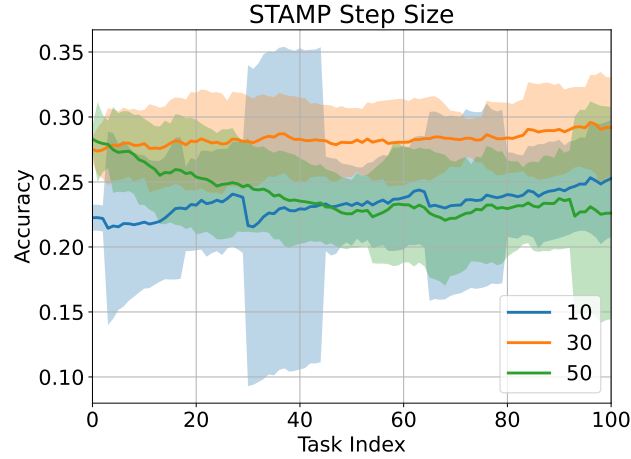


Figure 15: Analysis on different scheduling step size.

D.2.8 Gradient Matching Learning Rate

Figure 16 illustrates the effect of varying learning rates on the optimization of gradient matching. The results indicate that STAMP achieves optimal performance when the learning rate is set to 25.

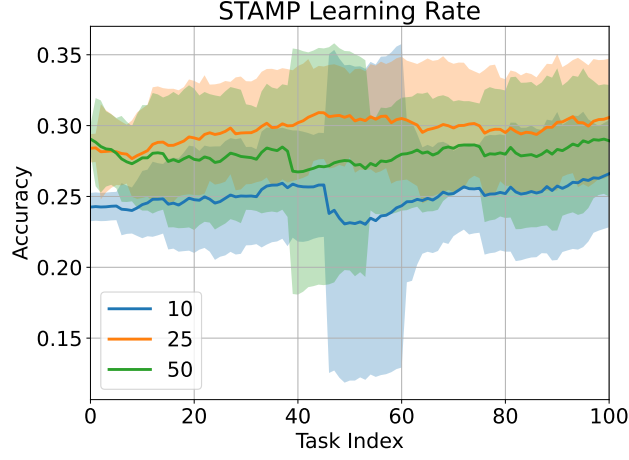


Figure 16: Analysis on different gradient matching learning rate.

D.2.9 Global Update Learning Rate

The global update learning rate significantly influences the norm of the aggregated gradient. As shown in Figure 17a, selecting a lower learning rate can reduce the norm of the aggregated gradient (see Figure 17b). This reduction may lead to slower convergence or result in gradient magnitudes that are insufficient to escape sharp minima.

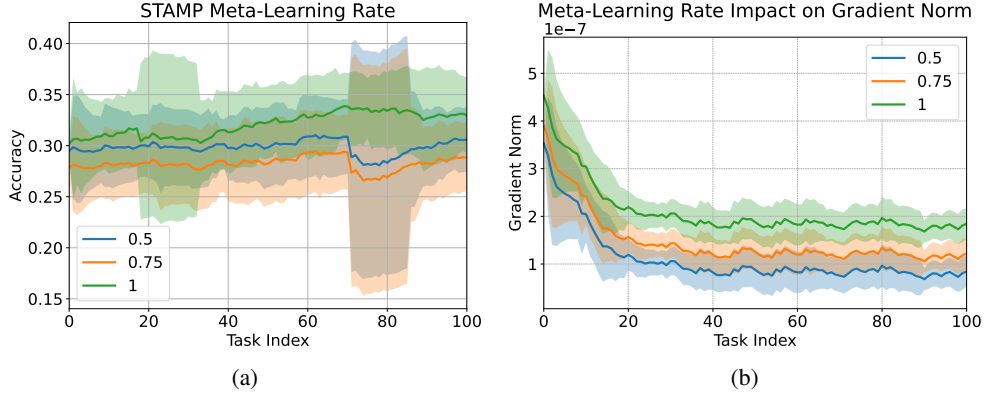


Figure 17: Analysis on global learning rate.

D.3 Effectiveness of Prototypical Coreset

Figure 18 illustrates the effectiveness of prototype learning from a prototypical coreset. This figure highlights two key observations: (1) the inability of vanilla FL to effectively learn prototypes from hidden representations, and (2) the improved prototype learning capability achieved by STAMP. In the case of FedAvg, the model fails to acquire sufficiently representative features due to the limitations imposed by the single-pass data stream.

In contrast, STAMP demonstrates strong class discrimination as it progresses through tasks, which enhances its ability to learn prototypes from a compact coreset. This improvement stems from the coreset selection process, which is guided by class-specific criteria. As a result, it reduces inter-class confusion that could otherwise lead to inaccurate or misleading prototype representations.

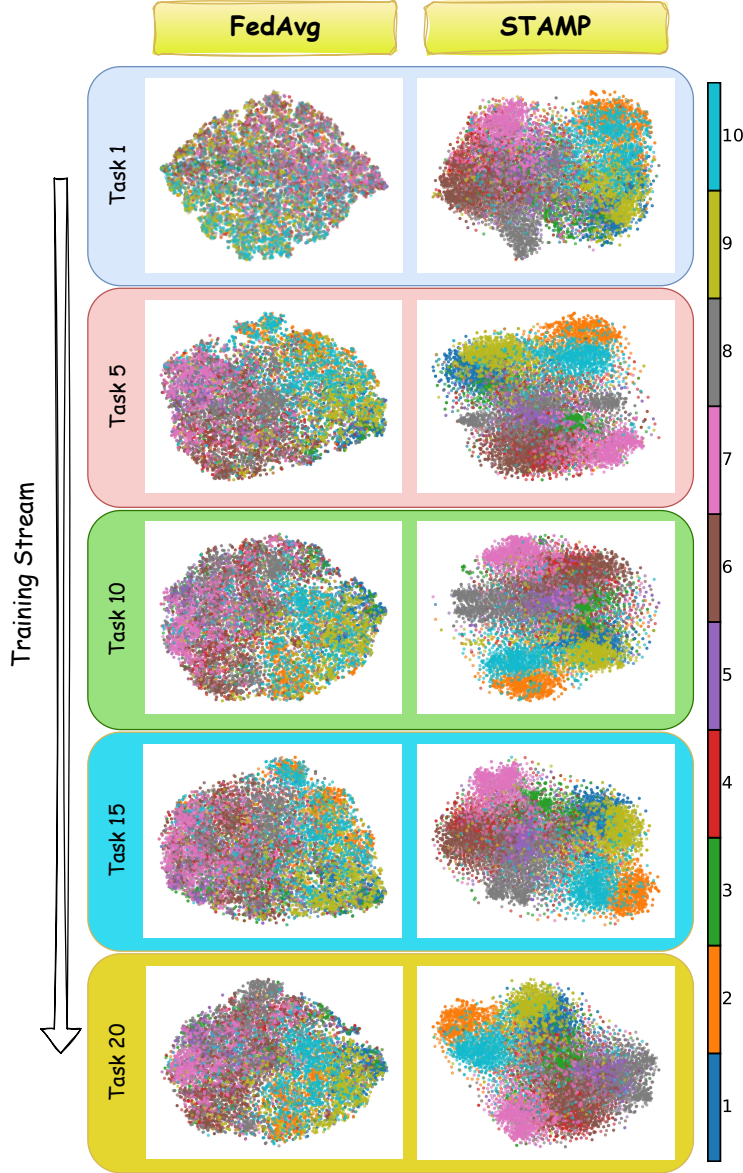


Figure 18: t-SNE visualizations of features learned by FedAvg and STAMP on the CIFAR-10 test set reveal notable differences. FedAvg exhibits significant class confusion when learning new classes, likely due to shortcut learning. In contrast, STAMP, leveraging a prototypical coreset, effectively mitigates forgetting and maintains clearer class separation.

E Privacy of STAMP

FL (McMahan et al., 2017), and FCL in particular, are vulnerable to various attacks such as data poisoning, model poisoning (Wan et al., 2024), backdoor attacks (Nguyen et al., 2023c), and gradient inversion attacks (Petrov et al., 2024; Balunovic et al., 2022; Dimitrov et al., 2022). Our proposed method does not introduce any additional privacy risks beyond those inherent to the standard FedAvg algorithm. Consequently, it is compatible with existing defense mechanisms developed for FedAvg, including secure aggregation () and noise injection prior to aggregation ().

Unlike several prior FCL approaches (Zhang et al., 2023a; Qi et al., 2023) that require clients to share either locally trained generative models or perturbed private data, STAMP relies solely on gradient matching. It utilizes the global model weights and the uploaded local model updates, information already exchanged among clients in the standard FedAvg setting, thus avoiding the need for additional private data sharing, especially over open communication environments (e.g., 5G/6G wireless networks).

F Limitations and Future Works

A primary limitation of our method lies in the sensitivity of gradient matching to the stability of task-wise and client-wise gradient trajectory approximation. Moreover, existing gradient matching approaches typically learn a single parameter set that adjusts the magnitude of task-specific gradients through a convex combination. Such approaches do not influence the direction of the gradients. Therefore, enhancing the stability of gradient trajectory approximation and improving gradient matching performance, particularly by extending the learnable parameter set to operate at the layer-wise or element-wise level, emerge as a promising direction for future research.